ACS OMEGA

http://pubs.acs.org/journal/acsodf

Article

Grafting a Porous Metal–Organic Framework [NH_2-MIL-101(Fe)] with AgCl Nanoparticles for the Efficient Removal of Congo Red

Qiyue Zhang, Aori Qileng, Jiale Li, Yiran Cao, Weipeng Liu, and Yingju Liu*

Cite This: *ACS Omega* 2023, 8, 4639–4648

Read Online

ACCESS | Metrics & More | Article Recommendations | Supporting Information

ABSTRACT: Organic dyes can produce harmful effects on the water environment, such as affecting the growth of aquatic organisms, reducing the transparency of water bodies, and causing eutrophication of water bodies, so it is necessary to mitigate the hazards of organic dyes. In this study, a metal–organic framework [NH_2-MIL-101(Fe)] was synthesized by the solvothermal method as a carrier for the in situ uniform deposition of AgCl nanoparticles on its surface, which was successfully used for both adsorption and degradation of Congo red. Adsorption results showed that the adsorption kinetics conformed to the proposed secondary adsorption kinetics equation with a maximum adsorption capacity of 248.4 $mg \cdot g^{-1}$. Furthermore, the degradation results indicated that with the aid of sodium borohydride as a reducing agent, the degradation of Congo red followed pseudo-first-order kinetics with a degradation rate of 0.077 min^{-1}, and the complete degradation of Congo red was finished within 18 min. Therefore, AgCl/NH_2-MIL-101(Fe) may find a potential application in the removal of dyes from wastewater.

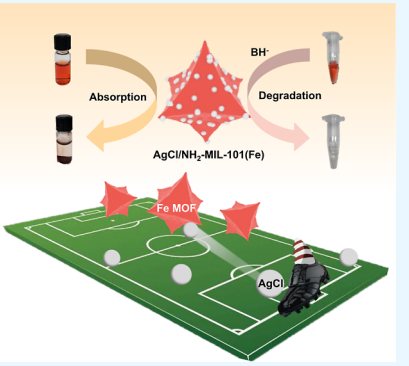

1. INTRODUCTION

Due to highly stable chemical properties, dyes are often used to color textiles and food products.[1] However, organic dye wastewater without complete or thorough treatment can cause potential pollution of water bodies.[2] Azo dyes, as one of the most commonly used class of organic dyes, contain one or more aromatic azo bonds (−N═N−) in the structure.[3] Azo dyes not only have the characteristics of toxicity, carcinogenesis, and mutation to human body but also resist biodegradation.[4] Congo red is a type of typical azo dye, while one of its metabolites, benzidine, is a known carcinogen that poses a serious health risk.[5] Traditional wastewater treatment methods such as photodegradation and biodegradation are unable to treat water contaminated with this dye.[6] Therefore, it is necessary to evanish the dye as far as possible before discharging the wastewater into the environment. However, traditional physicochemical treatment techniques such as chemical precipitation, reverse osmosis, and coagulation to remove dyes from wastewater are complex and time consuming.[7] On the contrary, the treatment of sodium borohydride ($NaBH_4$), a strong reductant, not only simplifies the procedure but also provides a comprehensive contaminant degradation. However, if only $NaBH_4$ was added without a catalyst, there was no significant degradation of the dye over a brief period.[8] Therefore, in view of minimizing the waste of resources and accelerating the degradation rate of dyes, it is necessary to develop a catalyst that can be combined with $NaBH_4$ to speed up the reaction rate.

Due to the self-assembly of organic connectors and metal nodes, metal–organic frameworks (MOFs) are network structures with the characteristics of high specific surface area and tunable pore size.[9] Herein, its comprehensive application has been found in catalysis for dye degradation, bio-oil refining and CO oxidation, and also adsorption for uranium, liquid dyes, and toxic gases.[10] In addition to improving the original structure, MOFs can be also modified by introducing other substances on their surface or inside to form composites that can enhance the effect of catalysis and dye adsorption.[11] For instance, Zhao et al. synthesized the three-dimensional MIL-125/g-C_3N_4 using the in situ growth, co-mingling, and lyophilization strategy, showing highly photocatalytic activity for the dyes,[12] while Nazir et al. synthesized ZIF-67 and ZIF-67 containing different Fe concentrations by the solvothermal method for the adsorption of rhodamine in water, displaying that the adsorption of ZIF-67 containing Fe was greater than that of ZIF-67.[13] Consequently, conventional MOFs can form composites with other substances that will be used both as adsorbents to adsorb pollutants and later to improve the efficiency of dye degradation. Among the reported types of MOFs, Fe-MOF can provide uniformly dispersed active sites to increase contact with dyes and reduce metal leaching to minimize environmental pollution.[14] Thus, a kind of Fe-MOF, NH_2-MIL-

Received: September 29, 2022
Accepted: January 18, 2023
Published: January 25, 2023

101(Fe), was selected as the support with other active materials for the adsorption and degradation application.

In recent years, silver halide (AgX, X = Cl, Br, I) has become a research focus in the field of catalysis because of its easy synthesis, good photosensitivity, and photocatalytic properties.[15] However, silver halide cannot escape the disadvantage of easy agglomeration to form a precipitate, which limits the practical application.[15] The NH_2-MIL-101(Fe) coordinated from 2-aminoterephthalic acid (NH_2-BDC) with $FeCl_3{\cdot}6H_2O$ contains a certain amount of Cl^-, so further treatment with $AgNO_3$ solution can deposit uniform AgCl nanoparticles (NPs) on the coordination sites of NH_2-MIL-101(Fe), which can not only avoid self-aggregation of AgCl[16] but also increase the specific surface area and active sites.

Herein, as in Scheme 1, the AgCl/NH_2-MIL-101(Fe) composite was synthesized and characterized by the structure

Scheme 1. Schematic Diagram of the FMA Composite for the Adsorption and Degradation of Congo Red

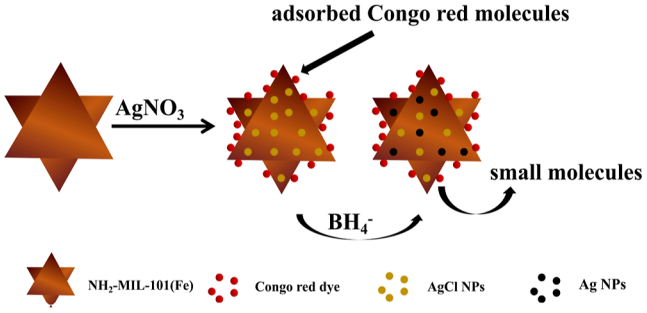

and the surface in detail. Due to the increased specific surface area and active sites, AgCl/NH_2-MIL-101(Fe) displayed a certain adsorption effect on Congo red. Additionally, AgCl/NH_2-MIL-101(Fe) displayed a rapid degradation of Congo red under the addition of $NaBH_4$, showing that $NaBH_4$ played roles in degrading Congo red, including reducing AgCl in situ to generate Ag NPs and also acting as an electron donor to provide electrons for catalytic hydrogenation and degradation of dyes. Thus, this work will provide an effective method for the removal of Congo red and the environmental reservation.

2. EXPERIMENTAL SECTION

2.1. Materials and Chemicals. $FeCl_3{\cdot}6H_2O$ was obtained from McLean Biochemical Technology Co., Ltd., Shanghai. NH_2-BDC, Congo red, and NaOH were purchased from Aladdin. Acetic acid, ethanol, *N*,*N*-dimethylformamide (DMF), and $AgNO_3$ were bought from Guangzhou Chemical Reagent Factory. Sodium anhydrous acetate was obtained from Guangdong Guanghua Chemical Factory Co, Ltd. $NaBH_4$ was bought from Tianjin Damao Chemical Reagent Factory.

2.2. Equipment. The morphology was characterized by transmission electron microscopy (TEM, Tecnai 12, FEI, Netherlands) and field emission scanning electron microscopy (SEM, FEI, Verios 460), while the powder diffraction patterns were performed by X-ray polycrystalline powder meter (XRD, Rigaku, Ulitma IV). The absorption spectrum was performed on a UV−visible spectrophotometer (UV-2250, Shimadzu), while the functional groups were characterized by Fourier transform infrared (FTIR) spectroscopy (Thermo Fisher, IS10). The specific surface area and pore size were acquired by an automatic multi-station specific surface and microporous mesoporous physical adsorption instrument (BET, MIKE, Gemini VII 2390). High resolution electrospray ionization mass spectroscopy (FT-MS, Bruker solanX 70, Agilent 6540TOF) was used to obtain the m/z of the degradation products. The elemental valence states were characterized by X-ray photoelectron spectroscopy (XPS, Thermo Scientific K-Alpha).

2.3. Solvothermal Synthesis of NH_2-MIL-101(Fe). The traditional solvothermal method was used to synthesize NH_2-MIL-101(Fe).[17] In simple terms, 0.675 g of $FeCl_3{\cdot}6H_2O$ (2.45 mM) and 0.225 g of NH_2-BDC (1.24 mM) were weighed and dispersed in 15 mL of DMF by sonication. Then, it was subsequently moved to a Teflon-lined autoclave (50 mL) and treated with heating at 110 °C for 20 h. After centrifuging, this reddish-brown solid was cleaned with deionized water, DMF, and ethanol twice in turn. After drying in a vacuum oven at 60 °C overnight, NH_2-MIL-101(Fe) was prepared.

2.4. Synthesis of AgCl/NH_2-MIL-101(Fe) (FMA). First, 20 mg of NH_2-MIL-101(Fe) was uniformly dispersed in 20 mL deionized water by ultrasonication. Second, 4 mL of $AgNO_3$ (100 mM) was dropwise added into the above solution and stirred for 1 min, while the color of the reaction solution changed to earthy yellow. After centrifuging and washing with deionized water and ethanol twice in turn, the product was placed overnight in a vacuum drying oven at 60 °C.

2.5. Batch Adsorption Tests. Simply, a stock solution of Congo red (1000 $mg{\cdot}L^{-1}$) with a dosage of 2 mg of FMA was prepared for the batch adsorption study. In the pH range of 5−11, the influence of pH on dye adsorption was investigated. Then, isothermal studies were performed by the adsorption of 43−871 $mg{\cdot}L^{-1}$ Congo red at pH = 6 and room temperature. After reaching adsorption equilibrium, a volume of the supernatant was taken out and the corresponding concentration was detected by measuring absorbance with a UV−vis spectrophotometer, which can reflect the remaining concentration of Congo red. The adsorption capacity (q_e) and removal (%) could be obtained by the following equations[18]

$$q_e = \frac{(C_0 - C_e)}{m} V \quad (1)$$

$$\text{removal}\ (\%) = \frac{C_0 - C_e}{C_0} \times 100 \quad (2)$$

where q_e is the adsorption amount at equilibrium ($mg{\cdot}g^{-1}$), m is the sorbent weight (g), V represents the solution volume (L), and C_0 and C_e represent the initial concentration ($mg{\cdot}L^{-1}$) and the remaining concentration ($mg{\cdot}L^{-1}$) of Congo red, respectively.

2.6. Catalytic Degradation Studies. In addition to its adsorption effect, FMA also enabled the rapid degradation of Congo red with the aid of $NaBH_4$. Catalytic degradation of Congo red by the FMA composite was investigated in the aqueous phase using $NaBH_4$ as the reducing agent, and the reaction degree corresponded to the change in absorbance of the characteristic peak of Congo red. First, $NaBH_4$ (150 mM, 50 μL) was mixed with Congo red (0.5 mM, 1 mL) in a neutral solution. Then, the FMA composite (1.5 $mg{\cdot}mL^{-1}$, 5 μL, total amount 7.5 μg) was put into the above solution and shaken gently to mix uniformly. During the reaction, the solution (50 μL) was taken out every 2 min and transferred to a quartz dish, and the UV−vis spectrum at the characteristic peak of Congo red (497 nm) was recorded to reflect the decolorization degree of the dye. When the characteristic peak

https://doi.org/10.1021/acsomega.2c06300
ACS Omega 2023, 8, 4639−4648

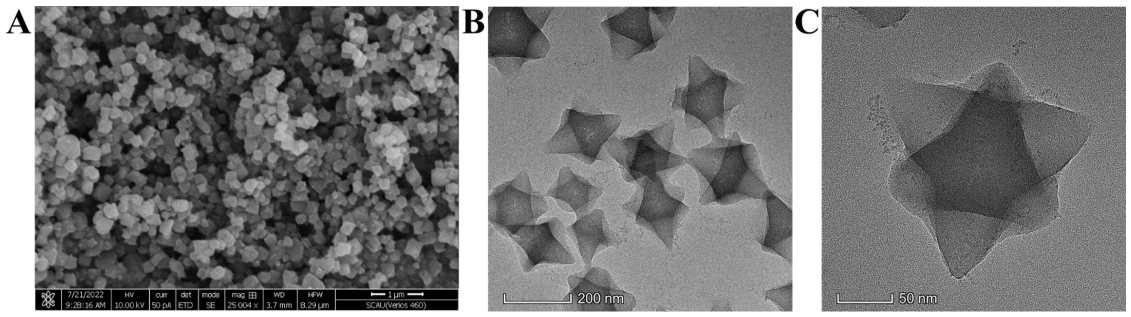

Figure 1. SEM image of NH_2-MIL-101(Fe) (A). TEM images of NH_2-MIL-101(Fe) at different magnifications (B,C).

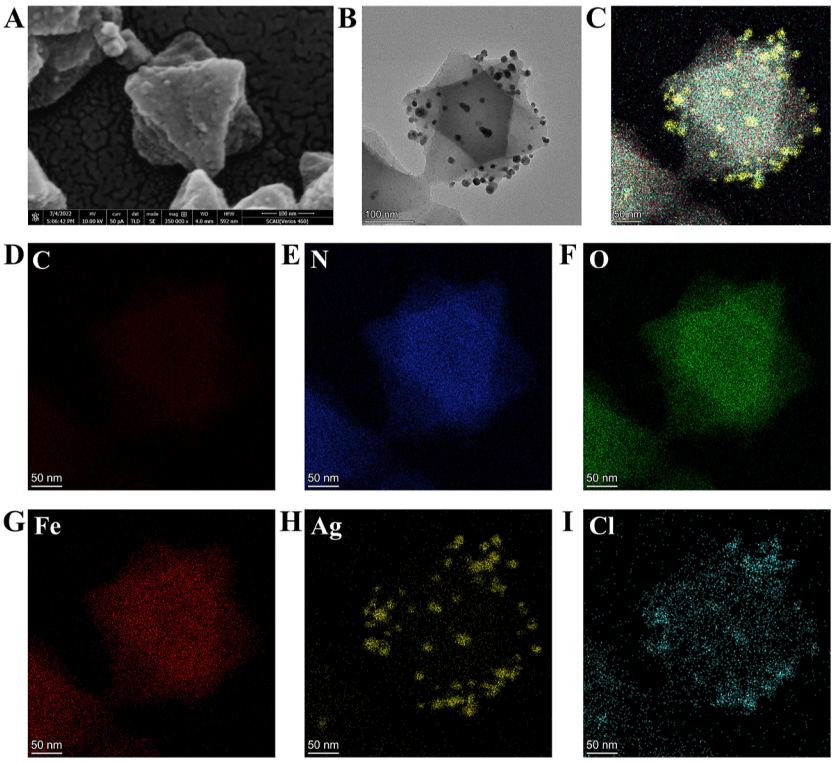

Figure 2. SEM (A), TEM (B), total elemental mapping (C) and single element mapping including C (D), N (E), O (F), Fe (G), Ag (H), and Cl (I) of the FMA composite.

at the UV−vis spectrum was no longer changed, the degradation reaction was completed.

3. RESULTS AND DISCUSSION

3.1. Surface Morphology Characterization. Figure 1A−C shows the SEM and the TEM images of NH_2-MIL-101(Fe), showing that NH_2-MIL-101(Fe) exhibited clear borders with uniform size distribution. After the deposition of AgCl NPs on NH_2-MIL-101(Fe) (Figure 2A−B), the FMA surface was decorated with a certain amount of tiny particles. In addition, the TEM elemental mapping of the FMA (Figure 2C−I) showed that the catalyst contained C, N, O, Fe, Ag, and Cl elements, where Fe, C, O, N, and Cl elements were derived from NH_2-MIL-101(Fe), and Ag originated from $AgNO_3$. Both Ag and Cl elements were synchronously dispersed, confirming the successful modification of AgCl NPs on the surface of NH_2-MIL-101(Fe). In this process, NH_2-MIL-101(Fe) performed two functions. First, it provided a porous structure so that it could adsorb dyes on its surface. Second, it also acted as a substrate material to distribute AgCl over its surface to avoid agglomeration into large particles. In addition, the FMA composite demonstrated good water dispersibility, which facilitated the study of dye adsorption and degradation.

The elemental valence states of the FMA composite were examined using XPS. It can be demonstrated from Figure 3A and Table S1 that the catalyst contained Ag, C, N, O, Fe, and Cl elements with 0.8, 67.5, 4.02, 23.85, 2.98, and 0.85%, respectively. In the C 1s region (Figure 3B), three characteristic peaks can be clearly seen, namely, C═O (288.7 eV), C−N (286.1 eV), and C−C (284.7 eV). In the Ag 3d region (Figure 3C), Ag can be observed in the chemical valence state as Ag^+, with two characteristic peaks at 367.3 and 373.3 eV corresponding to $3d_{5/2}$ and $3d_{3/2}$, respectively. The Fe 2p region (Figure 3D) can be fitted to four peaks, starting with two characteristic peaks attributed to Fe^{3+} at 711.5 and 725.4 eV, while the fitted peaks at 716.9 and 730.9 eV belonged to vibrational satellite peaks.

Then, FTIR spectroscopy was used to characterize the functional groups of NH_2-MIL-101(Fe) and the FMA composite, showing that the peaks of the FMA composite

https://doi.org/10.1021/acsomega.2c06300
ACS Omega 2023, 8, 4639−4648

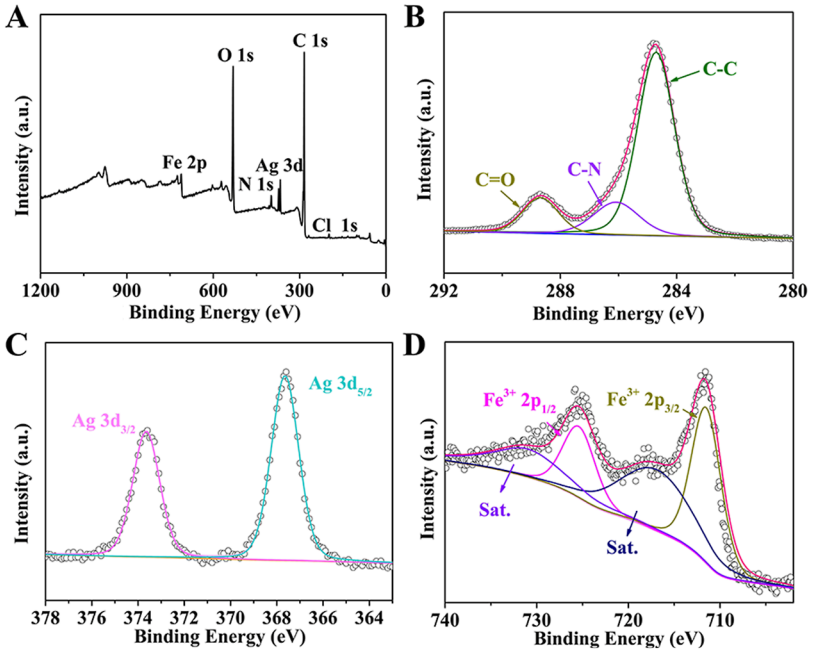

Figure 3. Survey spectrum of FMA (A) and deconvolution of C 1s (B), Ag 3d (C), and Fe 2p (D).

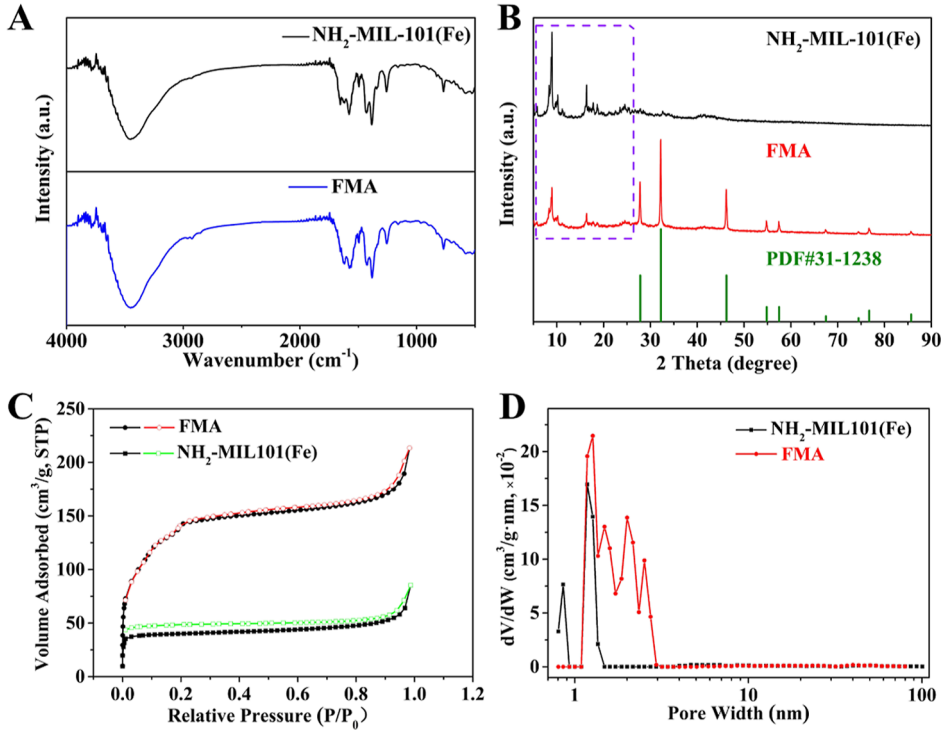

Figure 4. FTIR spectra (A), XRD (B), N_2 adsorption/desorption isotherms (C) and pore size distribution (D) of NH_2-MIL-101(Fe) and FMA.

(Figure 4A) were not significantly different from those of NH_2-MIL-101(Fe). Furthermore, the peaks of 1380, 1660, 1622, and 3451 cm^{-1} were all the characteristic peaks of the FMA composite. The peak of 3451 cm^{-1} was ascribed to the stretching vibration of N−H, while the peak of 1622 cm^{-1} was relevant to the bending vibration of N−H.[19] Additionally, the peaks at 1380 and 1660 cm^{-1} indicated −COO− and C═O groups.[20] These distinctive peaks of NH_2-MIL-101(Fe) did not change significantly after loading AgCl, suggesting that the deposition of AgCl in the FMA composite had no obvious effect on NH_2-MIL-101(Fe).

Next, the XRD patterns of NH_2-MIL-101(Fe) and FMA are shown in Figure 4B. Both of them displayed the same characteristic peaks at 5.08, 8.34, and 8.96°, which were ascribed to NH_2-MIL-101(Fe),[21] indicating the successful preparation of NH_2-MIL-101(Fe). The featured peaks for FMA at 57.42, 54.82, 46.20, 32.20, and 27.78° corresponded to the (222), (311), (220), (200), and (111) crystallographic planes of AgCl, respectively (PDF no. 31-1238). Therefore, the

https://doi.org/10.1021/acsomega.2c06300
ACS Omega 2023, 8, 4639−4648

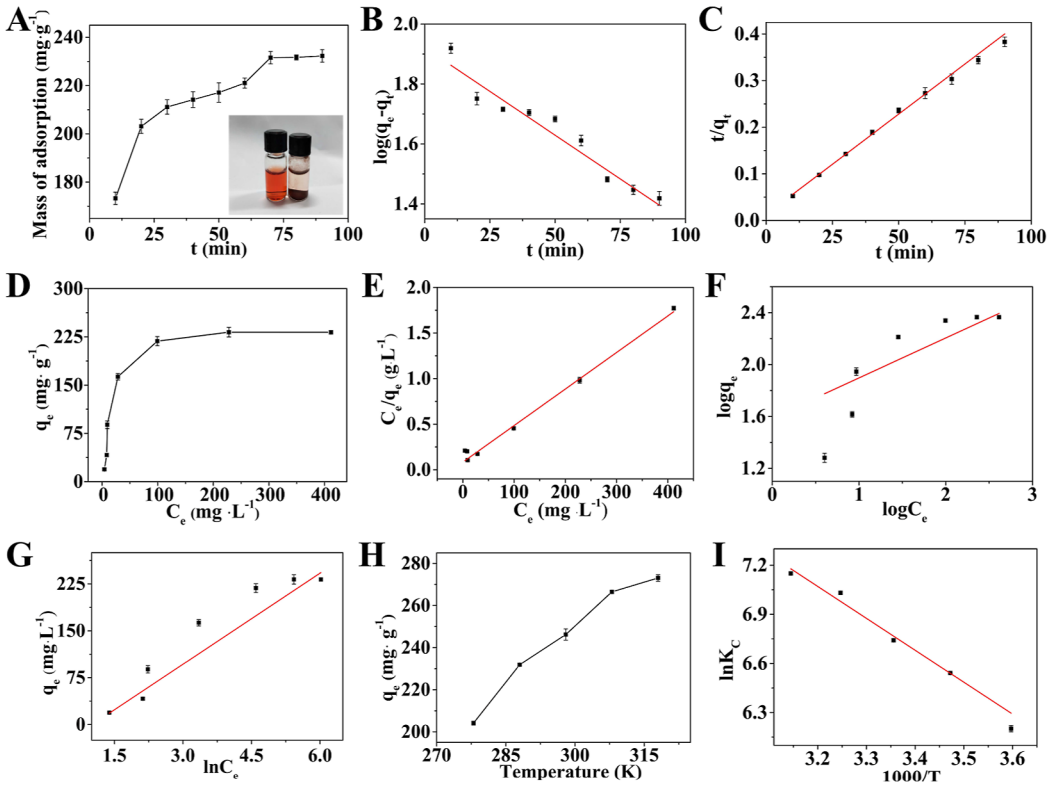

Figure 5. Adsorption kinetics of Congo red by FMA (A−C) (FMA amount = 2 mg; Congo red solution C_1 = 697 mg·L^{-1}; pH = 6; V_{tot} = 2 mL). Effect of the adsorption time on the adsorption amount (A) and the fitted first-order (B) and second-order (C) models. Adsorption isotherms of Congo red by FMA (D−G) (FMA amount = 2 mg; Congo red solution C_1 = 43−697 mg·L^{-1}; pH = 6; V_{tot} = 2 mL). The adsorption isotherm study on Congo red adsorption by FMA (D) and adsorption isotherms of Langmiur (E), Freundlich (F), and Tekin (G). Effect of the temperature on Congo red adsorption by the FMA (H) (FMA amount = 2 mg; Congo red solution C_1 = 697 mg·L^{-1}; pH = 6; V_{Tot} = 2 mL; T = 278−318 K) (H). Curve of ln(K_c) and 1000/T (I). The inset (A) shows the color change of Congo red before and after adsorption by the FMA composite.

successful preparation of the FMA catalyst was demonstrated, which was in agreement with the previous TEM characterization.

Finally, the pore size and the specific surface area of FMA and NH_2-MIL-101(Fe) were studied by the adsorption and desorption processes of nitrogen at 77 K. Figure 4C,D shows that the curve of NH_2-MIL-101(Fe) belonged to type IV isotherm and featured an H_3-type hysteresis loop, which was characteristic of a mesoporous material.[22] In contrast, the curve of FMA belonged to the mixed type I and type IV, implying the presence of both micropores and mesopores.[23] The Langmuir surface area of NH_2-MIL-101(Fe) was 202.31 m^2/g (BET, 126.44 m^2/g), while FMA exhibited a Langmuir surface area of 695.86 m^2/g (BET, 543.61 m^2/g); hence, the FMA composite possessed a larger surface area than NH_2-MIL-101(Fe), which could facilitate this catalyst to fully expose the active sites, improving the efficiency of dye adsorption and degradation. In addition, the FMA composite possessed more pore sizes compared to NH_2-MIL-101(Fe), since the deposition of AgCl NPs may form new pore sizes, which will provide more possibilities for the removal of Congo red.

3.2. Adsorption Study of Congo Red by the FMA Composite. The adsorption mechanism of the FMA composite for Congo red was investigated. Since pH was a major factor influencing the charge on the surface of materials, pH can affect the adsorption performance of materials for dyes.[24] Therefore, the capacity of the FMA composite to adsorb Congo red was investigated under different pH conditions. In Figure S1, when the pH increased from 5 to 11, the adsorption ability of the FMA composite gradually declined. As shown in Figure S2, under acidic conditions, the surface of the FMA composite was positively charged, while the Congo red belonged to the anionic dye, so it was more conducive to adsorption. However, under alkaline conditions, the FMA composite with a large number of negative charges on its surface produced the electrostatic repulsion with Congo red, resulting in a decrease in the adsorption rate.[25] In addition, the national standard for the pH of wastewater discharge is usually between 6 and 9 (GB8978-1996). Thus, the following adsorption experiments were performed at pH = 6.

3.2.1. Adsorption Kinetics Study. First, the adsorption ability of Congo red with time was studied by using the pseudo-first-order and pseudo-second-order kinetics as follows (eqs 3 and 4).[26]

$$\log(q_e - q_t) = \log q_e - K_1 t \tag{3}$$

$$\frac{t}{q_t} = \frac{1}{K_2 q_e^{\,2}} + \frac{t}{q_e} \tag{4}$$

where q_e is the adsorption amount for Congo red at the equilibrium state (mg·g^{-1}) and q_t is the actual adsorption amount for Congo red at time t (mg·g^{-1}). K_1 (min^{-1}) and K_2 (g·mg^{-1}·min^{-1}) are the adsorption rate constants of the proposed first-order and second-order models, respectively. As shown in Figure 5A, at the beginning of 30 min, the adsorption amount showed a sharp increase, which was due to the high

https://doi.org/10.1021/acsomega.2c06300
ACS Omega 2023, 8, 4639−4648

number of active sites on the FMA composite's surface. However, in 30−70 min, the adsorption amount still increased, but the rate slowed down. It might be because the active sites were occupied by a part of Congo red. Eventually, the adsorption rate gradually approached zero and the adsorption capacity reached a plateau. It could be seen from Figure 5B,C and Table S3 that the correlation coefficient of the proposed first-order kinetics relationship was R^2 = 0.903 and the correlation coefficient of the proposed second-order kinetics relationship was R^2 = 0.987, suggesting that the entire adsorption process was chemically controlled rather than free diffusion.[27] This may be a result of the increased transfer rate of Congo red and the rapid binding of Congo red to the active sites on the surface of FMA.[28] In addition, the second-order kinetics equation can provide a theoretical value of q_e as 232.6 mg·g^{-1} and K_2 as 4 × 10^{-3} (g·mg^{-1}·min^{-1}), while the actual adsorption capacity of q_e was 234.5 mg·g^{-1} according to eq 1; thus, the second-order kinetics was closer to the actual adsorption capacity. Furthermore, the adsorption rate of the FMA composite exhibited a more favorable adsorption rate, since the K_2 value was larger than 0.9 × 10^{-5} g·mg^{-1}·min^{-1} using a new uracil-modified chitosan adsorbent for Congo red by the four-step method.[29]

3.2.2. Adsorption Isotherm Study. To further study on the Congo red adsorption process by the FMA composite, the influence of the concentration of Congo red on the maximum adsorption capacity of the FMA composite was investigated. The linear fitting of the experimental data was performed, and the adsorption isotherm model for the adsorption process was determined by the fitting effect. Three models of Langmuir, Freundlich, and Temkin as follows were used (eqs 5−7).[30]

$$\frac{C_e}{q_e} = \frac{C_e}{q_{max}} + \frac{1}{K_L q_{max}} \tag{5}$$

$$\log q_e = \log K_F + \frac{1}{n}\log C_e \tag{6}$$

$$q_e = B\ \ln A + B\ \ln C_e \tag{7}$$

where C_e is the concentration of the dye at adsorption equilibrium (mg·L^{-1}), q_e is the adsorption amount at different concentrations (mg·g^{-1}), q_{max} is the maximum adsorption amount (mg·g^{-1}), K_L is the Langmuir constant, K_F is the Freundlich constant, and B is the Temkin constant. It could be seen from Figure 5D−G and Table S4 that the correlation coefficients (R^2) of the three models were 0.97, 0.64, and 0.96, respectively, indicating that the Langmuir model fitted better with the experimental data for the adsorption of Congo red.[31] It was consistent with the phenomenon that the adsorption increased rapidly and then slowly. The theoretical value of q_{max} and the Langmuir coefficient were 249.3 mg·g^{-1} and 0.047, respectively, by calculating from the slope and the intercept. Therefore, q_{max} was very approximated to the experimental maximum adsorption of 248.4 mg·g^{-1} from eq 1. In addition, the maximum adsorption of the FMA composite was a little larger than that of 128.6 mg·g^{-1} using $Fe_xCo_{3-x}O_4$ NPs for removing Congo red.[32]

3.2.3. Thermodynamic Investigation of Adsorption. After that, the influence of different temperatures on the adsorption was explored. In the thermodynamic experiments, the initial concentration of Congo red was 697 mg·L^{-1}, while the temperature was selected from 278 to 318 K. In Figure 5H, the Congo red adsorption by the FMA gradually increased at higher temperatures, which demonstrated that the adsorption of Congo red was an endothermic procedure; thus, an increasing temperature was beneficial to the adsorption. The following adsorption thermodynamics equations were used (eqs 8 and 9).[33]

$$\ln K_C = \frac{\Delta S}{R} - \left(\frac{\Delta H}{R}\right) \times \frac{1}{T} \tag{8}$$

$$\Delta G = \Delta H - T \times \Delta S \tag{9}$$

where R is the gas constant (8.314 J mol^{-1} k^{-1}), T is the Kelvin temperature, and K_C is the thermodynamic equilibrium constant. ΔS and ΔH can be acquired by calculating the intercept and the slope of the linear equation of ln K_C and $1/T$, respectively. The ΔG values were all negative from 278 to 318 K. In Figure 5I and Table S4, as the temperature increased, the ΔG showed a decreasing tendency, indicating that a higher temperature is more available for the adsorption. Meanwhile, a positive value of ΔH implied that the reaction was thermally driven, while a positive value of ΔS suggested that the FMA composite had an affinity toward the adsorption of Congo red.

3.3. Catalytic Degradation Study of Congo Red. Previously, the degradation of dyes required the addition of UV light[34] or the addition of *Pseudomonas aeruginosa*.[35] During the investigation of the adsorption mechanism of Congo red by the FMA composite, trace amounts of the FMA composite also had the ability to degrade the dye under the addition of $NaBH_4$. Therefore, the degradation process of Congo red dye by FMA was studied. First, in the pH range of 5−12, the influence of pH on the degradation of Congo red by the FMA composite was investigated. As shown in Figure S3, the absorbance of the degraded Congo red decreased gradually with the increase in pH. The Congo red failed to degrade completely at pH 5−6. The lower the pH, the higher the absorption peak of the remaining dye. When the pH was between 7 and 12, the absorbance of the Congo red was almost zero, indicating that the Congo red was completely degraded. The higher is the pH, the less the $NaBH_4$ is prone to self-hydrolysis.[36] Because the pH of the nationally allowed discharge wastewater was 6−9 and the absorbance of the dye at pH = 7 was closer to 0, pH = 7 was finally chosen for the follow-up study.

Second, the influence of $NaBH_4$ concentration in the range of 50−400 mM on Congo red degradation was investigated. The absorbance (Figure S4) of Congo red gradually decreased as the $NaBH_4$ concentration increased. When it reached 150 mM, the absorbance of Congo red remained almost unchanged. The $NaBH_4$ concentration was lower, and it can provide less BH_4^-; thus, it required a longer time to degrade the dye completely. The concentration of $NaBH_4$ was higher, and more amount of $NaBH_4$ remained after the complete degradation, which could release hydrogen by auto-hydrolysis. Thus, the final concentration of $NaBH_4$ was chosen as 150 mM.

By setting the volume of the FMA composite at 5 μL and the concentration range of the FMA composite from 0.5 to 4 mg·mL^{-1}, the effect of the FMA composite concentration on Congo red degradation was investigated. As shown in Figure S5, the absorbance of the Congo red gradually decreased with the increase in the FMA composite concentration. When the FMA composite concentration was 1.5 mg·mL^{-1}, the absorbance remained almost unchanged and it was almost completely decolorized. Further increase in the concentration

https://doi.org/10.1021/acsomega.2c06300
ACS Omega 2023, 8, 4639−4648

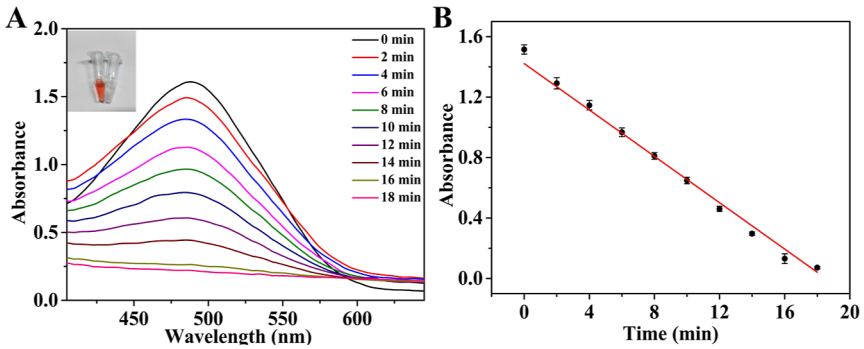

Figure 6. Time-dependent UV−vis absorption spectra of the degradation for Congo red (A) and plots of ln (C_t/C_0) vs time (B) (FMA solution C_0 = 1.5 mg·mL^{-1}, V_0 = 5 μL, FMA amount = 7.5 μg; Congo red solution C_1 = 0.5 mM; V_1 = 200 μL; $NaBH_4$ solution C_2 = 150 mM, V_2 = 10 μL; pH = 7; V_{tot} = 315 μL). The inset (A) shows the color change of Congo red before and after degradation by the FMA composite.

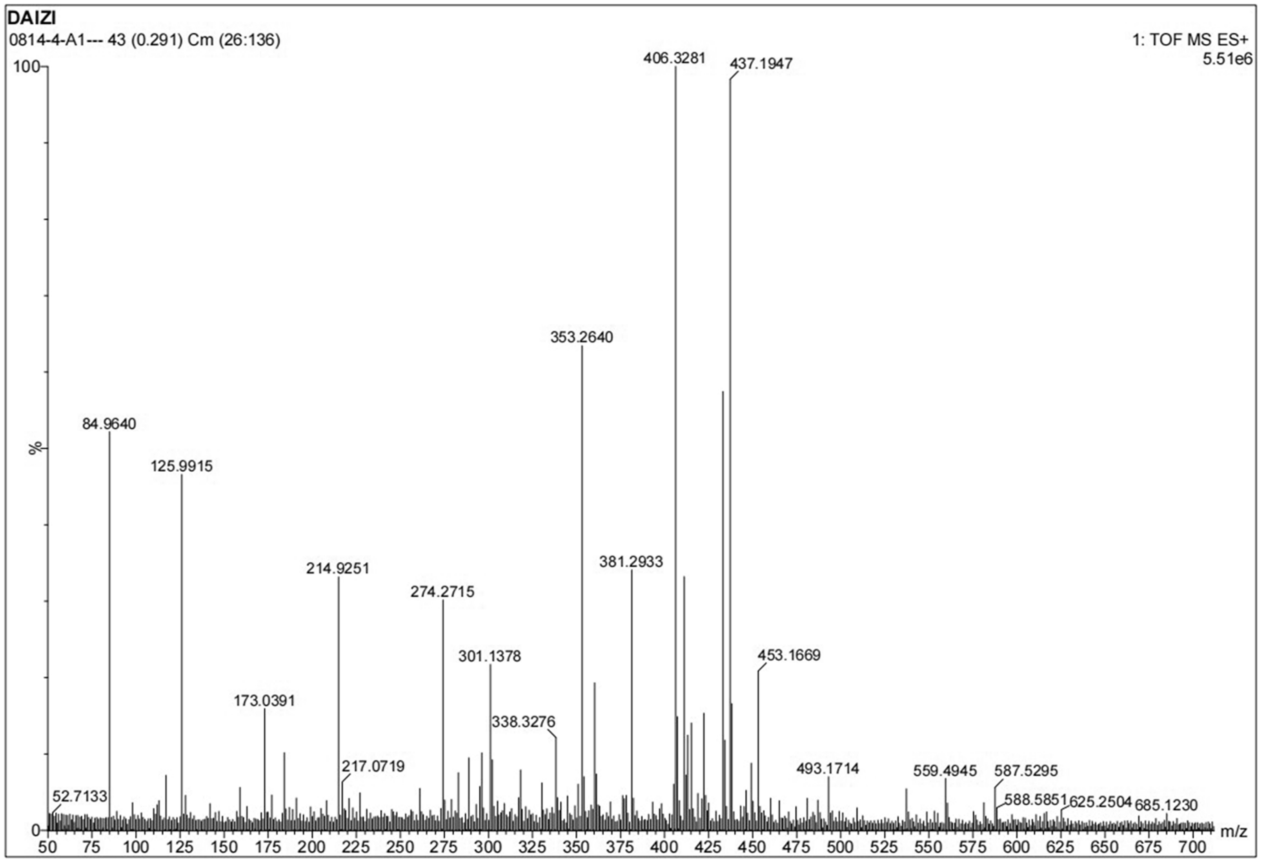

Figure 7. FT-MS spectra of the Congo red solution after the degradation.

of the catalyst from 1.5 to 4 mg·mL^{-1} can completely decolorize Congo red and eliminate the characteristic peak. Considering the cost of degradation, the final concentration of FMA was 1.5 mg·mL^{-1}.

Under optimal conditions, the absorbance changes of Congo red with time were investigated. The UV−vis characteristic peak (Figure 6A) for Congo red was mainly around 497 nm, and the absorbance decreased correspondingly as the reaction time increased. Once the reaction time was up to 18 min, the characteristic peak around 497 nm completely disappeared and the Congo red solution became colorless accordingly. The pseudo-first-order kinetics equation was further used to investigate the time-dependent curve of the degradation rate.[37]

$$\ln\left(\frac{C_t}{C_0}\right) = \ln\left(\frac{A_t}{A_0}\right) = -kt \quad (10)$$

where C_t is the dye concentration at time t, C_0 is the initial concentration of the dye, A_t is the dye absorbance at time t, A_0 is the initial dye absorbance, and k is the rate constant. As shown in Figure 6B, $\ln(A_t/A_0)$ had a good linear relationship with t, as $\ln(A_t/A_0) = -0.077t + 1.42$ (R^2 = 0.98), conforming to the pseudo-first-order kinetics. Among them, the degradation rate constant of Congo red was 0.077 min^{-1}, which was larger than 0.012 min^{-1} by using a chitosan−zirconia hybrid composite under visible light irradiation.[38] Therefore, the FMA was superior in degrading Congo red.

https://doi.org/10.1021/acsomega.2c06300
ACS Omega 2023, 8, 4639−4648

In addition, the intermediate products produced by the degradation of Congo red were characterized by FT-MS. According to the results in Figure 7, the degradation intermediates were mainly concentrated at an m/z of 437, 406, 353, 301, 215, and 173, which were quite different from the MS of pure Congo red (Figure S6). The possible structures of the intermediates in Figure 7 were analyzed and are provided in Figure S7, indicating a significant but not complete degradation of Congo red. From Figure S8, when the NH_2-MIL-101(Fe) was also used for Congo red degradation at the same conditions, the decolorization of Congo red by NH_2-MIL-101(Fe) was not significant. In addition, the only addition of $NaBH_4$ from Figure S9 or the only addition of FMA from Figure S10 showed an insignificant degradation after 18 min. Therefore, it can be indicated that both the surface-loaded AgCl and Ag NPs generated under the addition of $NaBH_4$ may play a function in dye degradation. Then, the XPS of the FMA after the addition of $NaBH_4$ was investigated. As shown in Figure S11, the valence states of Ag^+ and Ag^0 for the element Ag were discovered. Among them, 367.4 and 373.4 eV were characteristic peaks for Ag^+, while 368.1 and 374.1 eV were characteristic peaks for Ag^0, implying partial reduction of Ag^+ in AgCl to Ag NPs. Therefore, $NaBH_4$ played two main roles in degrading Congo red. It can reduce AgCl in situ to generate Ag NPs,[39] while it can also act as an electron donor to provide electrons for catalytic hydrogenation and degradation of dyes. In addition, the Ag NPs derived from the reduction of $NaBH_4$ were useful for accelerating Congo red degradation. Correspondingly, the possible degradation pathway of Congo red is the reduction of the azo group (−N═N−) to hydrazine group (−NH−NH−) using $NaBH_4$ as a reducing agent and FMA as a catalyst, resulting in the formation of $-NH_2-NH_2-$ and finally aromatic amino groups.[40,41]

In order to investigate the reusability of FMA, cycling tests were performed. As shown in Figure S12, the degradation rate decreased slightly in four cycles, and the final degradation efficiency was still as high as 82% in the fifth cycle of 18 min. The slight deceleration may be due to the residual intermediates adhering to the FMA surface. Therefore, FMA can exhibit its own recycling property and thus effectively reduce the cost in the degradation process.

4. CONCLUSIONS

The FMA composite was prepared by in situ depositing AgCl on NH_2-MIL-101(Fe) with high porosity and a large specific surface area. The FMA composite could be used not only for Congo red adsorption but also for Congo red degradation. Adsorption results showed that the adsorption kinetics conformed to the proposed secondary adsorption kinetics equation with a maximum adsorption capacity of 248.4 $mg \cdot g^{-1}$ within 90 min, while the FMA composite followed pseudo-first-order kinetics with the aid of $NaBH_4$ and exhibited good degradation performance against Congo red in 18 min. Herein, this work provided an effective method for wastewater treatment and a new insight into the application of MOFs. However, only a single dye was analyzed for adsorption and degradation, while the FMA composite for multiple dyes will be further investigated.

■ ASSOCIATED CONTENT

Supporting Information

The Supporting Information is available free of charge at https://pubs.acs.org/doi/10.1021/acsomega.2c06300.

Effect of pH on the adsorption of Congo red by the FMA; zeta potentials of FMA at different pH values; effect of pH on the degradation of Congo red by FMA; effect of the concentration of $NaBH_4$ on the degradation of Congo red; effect of the concentration of FMA on the degradation of Congo red; FT-MS spectra of the pure Congo red solution; possible pathway proposed for the degradation of Congo red; degradation of Congo red by only NH_2-MIL-101(Fe); degradation of Congo red by only $NaBH_4$; degradation of Congo red by only FMA; deconvolution of Ag of the FMA after the addition of $NaBH_4$; cycling degradation of the Congo red solution by FMA; element composition analysis of FMA; kinetics parameters of Congo red adsorption by FMA; isotherm parameters of Congo red adsorbed by FMA; and thermodynamic parameters of Congo red adsorption by FMA (PDF)

■ AUTHOR INFORMATION

Corresponding Author

Yingju Liu − *Key Laboratory for Biobased Materials and Energy of Ministry of Education, College of Materials and Energy, South China Agricultural University, Guangzhou 510642, China; Guangdong Provincial Key Laboratory of Agricultural & Rural Pollution Abatement and Environmental Safety, College of Natural Resources and Environment, South China Agricultural University, Guangzhou 510642, China;* orcid.org/0000-0002-1130-4945; Email: liuyingju@hotmail.com

Authors

Qiyue Zhang − *Key Laboratory for Biobased Materials and Energy of Ministry of Education, College of Materials and Energy, South China Agricultural University, Guangzhou 510642, China*

Aori Qileng − *Key Laboratory for Biobased Materials and Energy of Ministry of Education, College of Materials and Energy, South China Agricultural University, Guangzhou 510642, China*

Jiale Li − *Key Laboratory for Biobased Materials and Energy of Ministry of Education, College of Materials and Energy, South China Agricultural University, Guangzhou 510642, China*

Yiran Cao − *Key Laboratory for Biobased Materials and Energy of Ministry of Education, College of Materials and Energy, South China Agricultural University, Guangzhou 510642, China*

Weipeng Liu − *Key Laboratory for Biobased Materials and Energy of Ministry of Education, College of Materials and Energy, South China Agricultural University, Guangzhou 510642, China;* orcid.org/0000-0002-2153-1682

Complete contact information is available at: https://pubs.acs.org/10.1021/acsomega.2c06300

Notes

The authors declare no competing financial interest.

https://doi.org/10.1021/acsomega.2c06300
ACS Omega 2023, 8, 4639−4648

■ ACKNOWLEDGMENTS

This work was supported by the National Natural Science Foundation of China (22174059, 32170100), the Science and Technology Planning Project of Guangdong Province [2021B1212040008 (no.20210206)], the Educational Commission Foundation of Guangdong Province (2020ZDZX2025), and the Guangdong Basic and Applied Basic Research Foundation (2021A1515010208).

■ REFERENCES

(1) Raju, T. D.; Veeralingam, S.; Badhulika, S. Polyvinylidene Fluoride/$ZnSnO_3$ Nanocube/Co_3O_4 Nanoparticle Thermoplastic Composites for Ultrasound-Assisted Piezo-Catalytic Dye Degradation. *ACS Appl. Nano Mater.* **2020**, *3*, 4777−4787.

(2) Sun, Q.; Wu, K.; Zhang, J.; Sheng, J. W. Construction of $ZnFe_2O_4$/rGO Composites as Selective Magnetically Recyclable Photocatalysts under Visible Light Irradiation. *Nanotechnology* **2019**, *30*, 315706.

(3) Wang, B. W.; Wang, T. T.; Su, H. J. A Dye-methylene blue (MB)-degraded by Hydrodynamic Cavitation (HC) and Combined with Other Oxidants. *J. Environ. Chem. Eng.* **2022**, *10*, 107877.

(4) Basavarajappa, P. S.; Seethya, B. N. H.; Ganganagappa, N.; Eshwaraswamy, K. B.; Kakarla, R. R. Enhanced Photocatalytic Activity and Biosensing of Gadolinium Substituted $BiFeO_3$ Nanoparticles. *ChemistrySelect* **2018**, *3*, 9025−9033.

(5) Yang, Y. W.; Liu, K.; Sun, F. F.; Liu, Y. Y.; Chen, J. F. Enhanced Performance of Photocatalytic Treatment of Congo Red Wastewater by CNTs-Ag-Modified TiO_2 under Visible Light. *Environ. Sci. Pollut. Res.* **2022**, *29*, 15516−15525.

(6) Dehghani, M.; Nadeem, H.; Singh Raghuwanshi, V. S.; Mahdavi, H.; Banaszak Holl, M. M. B.; Batchelor, W. ZnO/Cellulose Nanofiber Composites for Sustainable Sunlight-Driven Dye Degradation. *ACS Appl. Nano Mater.* **2020**, *3*, 10284−10295.

(7) Lajevardi, A.; Tavakkoli Yaraki, M. T.; Masjedi, A.; Nouri, A.; Hossaini Sadr, M. H. Green Synthesis of MOF@Ag Nanocomposites for Catalytic Reduction of Methylene Blue. *J. Mol. Liq.* **2019**, *276*, 371−378.

(8) Rabbi, M. A.; Rahman, M. M.; Minami, H.; Habib, M. R.; Ahmad, H. Ag Impregnated Sub-micrometer Crystalline Jute Cellulose Particles: Catalytic and Antibacterial Properties. *Polymers* **2020**, *233*, 115842.

(9) Yu, Y.; Zhong, Y. C.; Xie, D.; Luo, G. Z.; Mao, Y. L.; Yuan, M. W.; Xiao, W. M.; Wang, S. H.; Chen, C. Fe_3O_4 Nanorods Coated with ZIF-8 and Decorated with Pt Nanoparticles as Magnetically Actuated Nanoscale Stirring Bars for Catalytic Dye Degradation, H_2 Production, and Hydrogenation of Olefins. *ACS Appl. Nano Mater.* **2021**, *4*, 10999−11006.

(10) Zhang, X.; Qiao, J.; Jiang, Y.; Wang, F.; Tian, X.; Wang, Z.; Wu, L.; Liu, W.; Liu, J. Carbon-Based MOF Derivatives: Emerging Efficient Electromagnetic Wave Absorption Agents. *Nano-Micro Lett.* **2021**, *13*, 135.

(11) Yang, S. L.; Karve, V. V.; Justin, A.; Kochetygov, I.; Espín, J.; Asgari, M.; Trukhina, O.; Sun, D. T.; Peng, L.; Queen, W. L. Enhancing MOF Performance through the Introduction of Polymer Guests. *Chem. Rev.* **2021**, *427*, 213525.

(12) Zhao, J.; Li, B. Z.; Liu, Z. Y.; Dai, D. L.; Li, Y. Q.; Shi, R. H.; Zhang, H. A Novel Solar-Triggered MIL-125(Ti)/g-C_3N_4/SA Composite Aerogel with High Catalytic Activity for Degradation of Organic Contaminants Sep. *Purif. Technol.* **2021**, *279*, 119696.

(13) Nazir, M. A.; Bashir, M. S.; Jamshaid, M.; Anum, A.; Najam, T.; Shahzad, K.; Imran, M.; Shah, S. S. A.; Rehman, A. U. Synthesis of Porous Secondary Metal-Doped MOFs for Removal of Rhodamine B from Water: Role of Secondary Metal on Efficiency and Kinetics. *Surf. Interfaces* **2021**, *25*, 101261.

(14) Han, X. L.; Zhang, W.; Li, S.; Cheng, C. Y.; Zhou, L.; Jia, Q. L.; Xiu, G. L. Efficient Activation of Peroxymonosulfate by MnS/Fe-MOF Hybrid Catalyst for Sulfadiazine Degradation: Synergistic Effects and Mechanism. *Purif. Technol.* **2022**, *287*, 120509.

(15) Liu, W. T.; Chen, D. L.; Yoo, S. H.; Cho, S. O. Hierarchical Visible-Light-Response Ag/AgCl@TiO_2 Plasmonic Photocatalysts for Organic Dye Degradation. *Nanotechnology* **2013**, *24*, 405706.

(16) Gong, J. Q.; Zhang, W. W.; Sen, T.; Yu, Y. C.; Liu, Y. C.; Zhang, J. L.; Wang, L. Z. Metal-Organic Framework MIL-101(Fe) Nanoparticles Decorated with Ag Nanoparticles for Regulating the Photocatalytic Phenol Oxidation Pathway for Cr(VI) Reduction. *ACS Appl. Nano Mater.* **2021**, *4*, 4513−4521.

(17) Jiang, Z. W.; Gao, P. F.; Yang, L.; Huang, C. Z.; Li, Y. F. Facile in Situ Synthesis of Silver Nanoparticles on the Surface of Metal-Organic Framework for Ultrasensitive Surface-Enhanced Raman Scattering Detection of Dopamine. *Anal. Chem.* **2015**, *87*, 12177−12182.

(18) Zhang, Y. M.; Zhao, S. J.; Mu, M.; Wang, L. S.; Fan, Y.; Liu, X. F. Eco-Friendly Ferrocene-Functionalized Chitosan Aerogel for Efficient Dye Degradation and Phosphate Adsorption from Wastewater. *Chem. Eng. J.* **2022**, *439*, 135605.

(19) Liu, M.; Huang, Q. L.; Li, L.; Zhu, G. P.; Yang, X. J.; Wang, S. X. Cerium-doped MIL-101-NH_2(Fe) as Superior Adsorbent for Simultaneous Capture of Phosphate and As(V) from Yangzonghai Coastal Spring Water. *J. Hazard. Mater.* **2022**, *423*, 126981.

(20) Li, X.; Zheng, H. Y.; Chen, J. H.; Xu, M. Y.; Bai, Y.; Liu, T. T. MIL-101(Fe)@Ag Rapid Synergistic Antimicrobial and Biosafety Evaluation of Nanomaterials. *Molecules* **2022**, *27*, 3497.

(21) Li, X. H.; Guo, W. L.; Liu, Z. H.; Wang, R. Q.; Liu, H. Quinone-Modified NH_2-MIL-101(Fe) Composite as a Redox Mediator for Improved Degradation of Bisphenol A. *J. Hazard. Mater.* **2017**, *324*, 665−672.

(22) Bagherzadeh, S. B.; Kazemeini, M.; Mahmoodi, N. M. Preparation of Novel and Highly Active Magnetic Ternary Structures (Metal-Organic Framework/Cobalt Ferrite/Graphene Oxide) for Effective Visible-Light-Driven Photocatalytic and Photo-Fenton-Like Degradation of Organic Contaminants. *J. Colloid Interface Sci.* **2021**, *602*, 73−94.

(23) Dong, W.; Chen, G.; Hu, X.; Zhang, X.; Shi, W.; Fu, Z. Molybdenum Disulfides Nanoflowers Anchoring Iron-Based Metal Organic Framework: A Synergetic Catalyst with Superior Peroxidase-Mimicking Activity for Biosensing. *Sens. Actuators, B* **2020**, *305*, 127530.

(24) Yuan, Z. Y.; Wang, J.; Wang, Y. M.; Liu, Q.; Zhong, Y. J.; Wang, Y.; Li, L.; Lincoln, S. F.; Guo, X. H. Preparation of a Poly(acrylic acid) Based Hydrogel with Fast Adsorption Rate and High Adsorption Capacity for the Removal of Cationic Dyes. *RSC Adv.* **2019**, *9*, 21075−21085.

(25) Ain, Q.; Rasheed, U.; Yaseen, M.; Zhang, H. B.; Tong, Z. F. Superior Dye Degradation and Adsorption Capability of Polydopamine Modified Fe_3O_4-Pillared Bentonite Composite. *J. Hazard. Mater.* **2020**, *397*, 122758.

(26) Khosravi-Nikou, M. R.; Safari, M. H.; Rad, A. A.; Hassani, P.; Mohammadian, M.; Ahmadi, M.; Ghafari, N.; Naseri, M. Desulfurization of Liquid Fuels Using Aluminum Modified Mesoporous Adsorbent: towards Experimental and Kinetic Investigations. *Sci. Rep.* **2021**, *11*, 8848.

(27) Zhang, X. N.; Lin, X. Y.; He, Y.; Chen, Y.; Zhou, J.; Luo, X. G. Adsorption of Phosphorus from Slaughterhouse Wastewater by Carboxymethyl Konjac Glucomannan Loaded with Lanthanum. *Int. J. Biol. Macromol.* **2018**, *119*, 105−115.

(28) Basha, I. K.; Abd El-Monaem, E. M.; Khalifa, R. E.; Omer, M.; Eltaweil, A. S. Sulfonated Graphene Oxide Impregnated Cellulose Acetate Floated Beads for Adsorption of Methylene Bue Dye: Optimization Using Response Surface Methodology. *Sci. Rep.* **2022**, *12*, 9339.

(29) Al-Harby, N. F.; Albahly, E. F.; Mohamed, N. A. Synthesis and Characterization of Novel Uracil-Modified Chitosan as a Promising Adsorbent for Efficient Removal of Congo Red Dye. *Polymers* **2022**, *14*, 271.

(30) Gomaa, H.; Abd El-Monaem, E. M.; Eltaweil, A. S.; Omer, A. M. Efficient Removal of Noxious Methylene Blue and Crystal Violet

https://doi.org/10.1021/acsomega.2c06300
ACS Omega 2023, 8, 4639−4648

Dyes at Neutral Conditions by Reusable Montmorillonite/$NiFe_2O_4$@ Amine-Functionalized Chitosan Composite. *Sci. Rep.* **2022**, *12*, 15499.
(31) Hassan, M. M.; Carr, C. M. A Critical Review on Recent Advancements of the Removal of Reactive Dyes from Dyehouse Effluent by Ion-Exchange Adsorbents. *Chemosphere* **2018**, *209*, 201−219.
(32) Liu, J.; Wang, N.; Zhang, H. L.; Baeyens, J. Adsorption of Congo Red Dye on Fe_xCo_3-xO_4 Nanoparticles. *J. Environ. Manage.* **2019**, *238*, 473−483.
(33) Ru, J.; Wang, X. M.; Wang, F. B.; Cui, X. L.; Du, X. Z.; Lu, X. Q. UiO Series of Metal-Organic Frameworks Composites as Advanced Sorbents for the Removal of Heavy Metal Ions: Synthesis, Applications and Adsorption Mechanism. *Ecotoxicol. Environ. Saf.* **2021**, *208*, 111577.
(34) Bartkus, T. P.; T'ien, J. S.; Sung, C. J. A Semi-Global Reaction Rate Model Based on Experimental Data for the Self-Hydrolysis Kinetics of Aqueous Sodium Borohydride. *Int. J. Hydrogen Energy* **2013**, *38*, 4024−4033.
(35) Shah, N. S.; Khan, J. A.; Sayed, M.; Khan, Z. U. H.; Iqbal, J.; Arshad, S.; Junaid, H. M.; Khan, H. M. Synergistic Effects of H_2O_2 and $S_2O_8^{2-}$ in The Gamma Radiation Induced Degradation of Congo-Red Dye: Kinetics and Toxicities Evaluation. *Sep. Purif. Technol.* **2020**, *233*, 115966.
(36) Shanmugam, B. K.; Easwaran, S. N.; Mohanakrishnan, A. S.; Kalyanaraman, C.; Mahadevan, S. Biodegradation of Tannery Dye Effluent using Fenton's Reagent and Bacterial Consortium: A Biocalorimetric Investigation. *J. Environ. Manage.* **2019**, *242*, 106−113.
(37) Thor, S.-H.; Ho, L.-N.; Ong, S.-A.; Abidin, C. Z. A.; Heah, C.-Y.; Nordin, N.; Ong, Y.-P.; Yap, K.-L. Discovering the Roles of Electrode Distance and Configuration in Dye Degradation and Electricity Generation in Photocatalytic Fuel Cell Integrated Electro-Fenton Process. *Sep. Purif. Technol.* **2022**, *278*, 119652.
(38) Das, R. S.; Kumar, A.; Wankhade, A. V.; Peshwe, D. R. ZrO_2@ Chitosan Composite for Simultaneous Photodegradation of Three Emerging Contaminants and Antibacterial Application. *Carbohydr. Polym.* **2022**, *278*, 118940.
(39) Qin, Y. Z.; Mo, F.; Yao, S.; Wu, Y. Z.; He, Y. S.; Yao, W. X. Facile Synthesis of Porous Ag Crystals as SERS Sensor for Detection of Five Methamphetamine Analogs. *Molecules* **2022**, *27*, 3939.
(40) Khan, S. A.; Mohammed, S. A.; Bakhsh, E. M.; Al-Ghamdi, Y. O.; Rauf, A.; Akhtar, K.; Begum, A.; Khan, S. B. Reduction of Nitrophenol Isomers and Degradation of Azo Dyes through Zero-Valent Ni Nanoparticles Anchored on Cellulose Acetate Coated Ce/Zr Composite. *J. Water Proc. Eng.* **2021**, *44*, 102383.
(41) Liu, J.; Liu, A.; Li, J.; Liu, S. T.; Zhang, W. X. Probing the Performance and Mechanisms of Congo Red Wastewater Decolorization with Nanoscale Zero-valent Iron in the Continuing Flow Reactor. *J. Cleaner Prod.* **2022**, *346*, 131201.

https://doi.org/10.1021/acsomega.2c06300
ACS Omega 2023, 8, 4639−4648